Auger cascades in resonantly excited neon

S. Stock,* R. Beerwerth, and S. Fritzsche
Helmholtz Institute Jena, Fröbelstieg 3, 07743 Jena, Germany
and Theoretisch-Physikalisches Institut, Friedrich-Schiller-Universität Jena, 07743 Jena, Germany
(Received 23 March 2017; published 16 May 2017)

The Auger cascades following the resonant $1s \rightarrow np$ ($n = 3,4$) excitation of neutral neon are studied theoretically. In contrast to previous investigations, we here model the complete cascade from the initially core-excited $1s^{-1}3p\ ^1P_1$ and $1s^{-1}4p\ ^1P_1$ levels of Ne up to the doubly ionized Ne^{2+} ions. Extensive multiconfiguration Dirac-Fock calculations are carried out, combined with a proper cascades model, to incorporate as many decay branches as possible, including all major single-electron shake-up and shake-down processes. We simulate the electron spectra and predict shake probabilities, ion yields, as well as the relative population of the intermediate and final states. Experimentally known level energies for neutral, singly, and doubly ionized neon are utilized whenever possible in order to improve the predictions. Most features from experiment can be reproduced with quite good agreement if a sufficiently large basis is taken into account. These simulations therefore demonstrate not only the required computational effort, but also that it is nowadays possible to predict whole Auger spectra of decay cascades, a central feature for further exploring electron coincidence maps as obtained at synchrotrons and free-electron lasers.

DOI: 10.1103/PhysRevA.95.053407

I. INTRODUCTION

Auger electron spectroscopy has been found a versatile tool for studying the electronic structure of atoms and molecules. In particular, the autoionization of inner-shell excited or ionized noble gases has been investigated extensively in the past decades [1–9]. Apart from plasma and astrophysics, such autoionization studies are of fundamental interest to better understand the dynamics of atoms and molecules in intense radiation fields.

Double and even multiple autoionization of atoms is often possible if an inner-shell vacancy is created. Such a double Auger (DA) process was first detected in 1965 [1]. Generally, two different and competing DA mechanisms are distinguished, namely the (so-called) *direct* and *cascade* DA. While the direct DA process is a high-order process in which both electrons share the (transition) energy and are ejected simultaneously [10], a subsequent electron emission occurs in the cascade DA process. In good approximation, the cascade DA decay can be described by a two-step process in which the first step still leads to an autoionizing state that can decay by further electron emission. Usually, a DA process is a combination of both direct and cascade processes [9]. For medium and heavy atoms, moreover, inner-shell excitations often result even in triple or multiple ionization [11]. Recently, even a *direct triple* Auger decay was observed for the first time [12]. To describe such direct processes, the shake-off and knock-out mechanisms have been proposed [13,14].

Auger cascades have been studied extensively, both experimentally and theoretically [15–19]. In particular, if a $1s$ electron of a nearly neutral atom is excited to an otherwise empty np shell, such cascades frequently proceed via *spectator* processes, in which the excited valence-shell electron itself does not participate in the autoionization in the first step. Therefore, the ions are often left in an autoionizing state and then undergo a second Auger decay. For such electron emission cascades, shake processes are known to play an essential role [2–4,6,8] and require special care in any theoretical description.

Although the Auger electron spectra of $1s \rightarrow 3p$ and $1s \rightarrow 4p$ excited neon have been explored experimentally [3,5,6,8,15–17,20], a detailed numerical simulation of the overall two-step Auger cascades is still missing at present. In this work, we therefore investigate the single and double autoionization of neon atoms with an initial K-shell hole, following the resonant $1s \rightarrow 3p$ and $1s \rightarrow 4p$ photoexcitation. For these cascades, we performed extensive multiconfiguration Dirac-Fock (MCDF) computations in which all major single-electron shake-up and shake-down processes are incorporated systematically into the calculation of the Auger rates for all possible decay paths. Our approach is conceptually similar to that of Kochur *et al.* [21–24] to the effect that we aim to construct complete deexcitation trees starting from an initial vacancy. However, since we are carrying out calculations for all possible Auger decays between fine-structure levels, we are able to simulate detailed Auger electron spectra. As far as available, we compare our results to experiments and find good agreement for our simulated spectra as well as for shake probabilities and ion yields.

Our paper is structured as follows: In Sec. II, we first introduce in detail the two Auger cascades following the inner-shell excitation of the $1s^{-1}3p\ ^1P_1$ and $1s^{-1}4p\ ^1P_1$ levels of neon, respectively, which are the focus of this work. Here, we also briefly outline the MCDF method as well as the biorthonormal transformation that is used in evaluating the Auger amplitudes and rates. Section III then describes further details about the generation of the systematically enlarged wave functions, and how we make use of experimental energies to further improve the simulated spectra. Our results are discussed in Sec. IV which is subdivided into two parts, one which addresses the first step of the cascade as well as the shake probabilities and ion yields, and another part in which the second step of the cascade and the population of the final

*sebastian.stock@uni-jena.de

states are discussed. Finally, a short summary of our findings is given in Sec. V.

II. THEORY

A. Auger cascades after inner-shell excitation

In neutral neon, the resonant photoexcitation of a $1s$ electron leads to the core-excited $1s^{-1}3p\ ^1P_1$ level at the (well-known) photon energy 867.13 eV, or to the $1s^{-1}4p\ ^1P_1$ level at 868.76 eV [25]. In comparison, the photoexcitation of the neighboring $1s^{-1}np\ ^3P$ levels from the $^1S_0$ ground state is typically suppressed by a factor of about 10^{-3}. Therefore, we here restrict ourselves to the Auger cascades of the initially excited $1s^{-1}np\ ^1P_1$ levels.

There are two major steps in the cascade decay of $1s^{-1}np\ ^1P_1$ core-excited neon atoms. In a first step, these atoms emit a fast Auger electron within $\approx$3 fs and become Ne^+ ions with a hole in either the $2s$ or $2p$ shell. For this first step of the cascade, we shall take into account all those levels that can be reached by spectator *or* participator decays as well as by single-electron shake-up or shake-down processes of the initially excited $3p$ or $4p$ electron. In addition to the two electrons that *normally* participate in any Auger decay, i.e., the deexcited and the emitted electron, in single-electron shake processes, a third electron is displaced from its shell into a higher subshell (*shake-up*) or a lower one (*shake-down*). If, moreover, the (shaken) electron changes its orbital angular momentum, we refer to this as a *conjugate* shake process. In the first step of the cascades, we here include all shake processes of the initially excited $3p$ or $4p$ spectator electron to any of the np subshells with $n = 3, \ldots, 7$, as well as conjugate shake transitions to the $3d$ subshell. Therefore, the first step of the Auger cascades above can be summarized as

$$\mathrm{Ne}\ 1s^{-1}np\ ^1P_1 \rightarrow \mathrm{Ne}^+ \left\{ \begin{array}{c} 1s^2 2s^2 2p^5 \\ 1s^2 2s^1 2p^6 \\ 1s^2 2s^2 2p^4 n'\ell \\ 1s^2 2s^1 2p^5 n'\ell \\ 1s^2 2s^0 2p^6 n'\ell \end{array} \right\} + e^- . \qquad (1)$$

Some of the final states on the right-hand side of step (1) are still autoionizing since they lie above the double-ionization threshold. These final states of the first step then become the *initial* states of the second step of the Auger cascade, in which electrons with much lower energy are emitted. For this second step of the cascade, we include all final states that arise from the $2s^2 2p^4$ and $2s^1 2p^5$ configurations, as well as several energetically allowed levels from the $2s^2 2p^3 n\ell$ configurations:

$$\begin{aligned} &\mathrm{Ne}^+\ 1s^2 2s^2 2p^4 n\ell \rightarrow \mathrm{Ne}^{2+}\ 1s^2 2s^2 2p^4 + e^- , \\ &\mathrm{Ne}^+\ 1s^2 2s^1 2p^5 n\ell \rightarrow \mathrm{Ne}^{2+} \left\{ \begin{array}{c} 1s^2 2s^2 2p^4 \\ 1s^2 2s^1 2p^5 \end{array} \right\} + e^- , \\ &\mathrm{Ne}^+\ 1s^2 2s^0 2p^6 n\ell \rightarrow \mathrm{Ne}^{2+} \left\{ \begin{array}{c} 1s^2 2s^1 2p^5 \\ 1s^2 2s^2 2p^4 \\ 1s^2 2s^2 2p^3 n'\ell' \end{array} \right\} + e^- . \end{aligned} \qquad (2)$$

In addition to the shake transitions of the $n\ell$ valence electron, as mentioned above, we here included also the conjugate $2p \rightarrow 2s$ shake-down displacements in order to account for the energetically allowed Auger transitions between the fine-structure levels of the $2s^0 2p^6 n\ell \rightarrow 2s^2 2p^4$ and $2s^0 2p^6 n\ell \rightarrow 2s^2 2p^3 n'\ell'$ configurations, respectively.

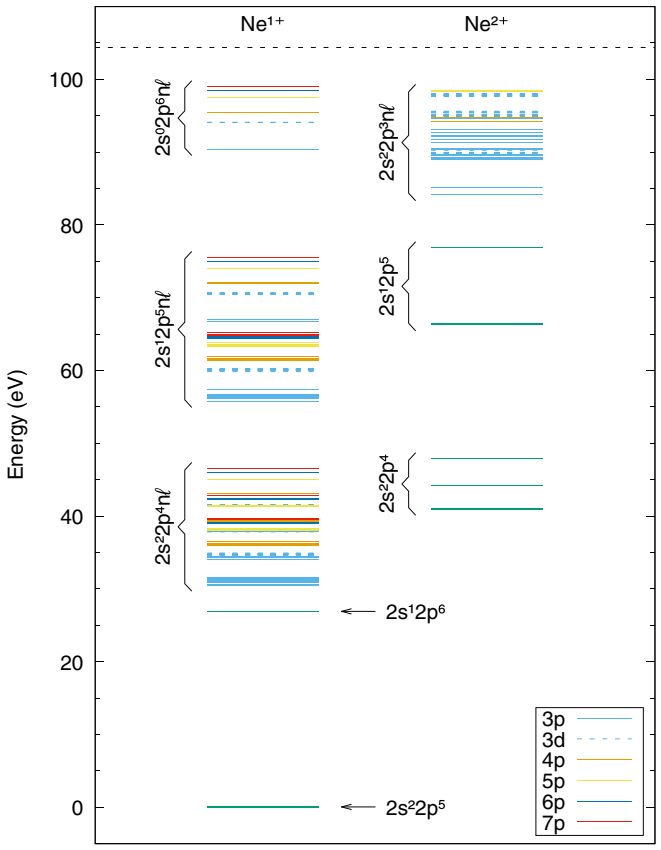

FIG. 1. Energy levels of Ne^+ and Ne^{2+} ions relative to the $1s^2 2s^2 2p^5\ ^2P_{3/2}$ ground level of Ne^+. Only the levels that are relevant for the cascade as outlined in Eqs. (1) and (2) are shown. Here, we employed experimental level energies whenever available and interpolated the energies of the remaining levels based on experimentally observed levels; cf. Sec. III B. The dashed line at 104.4 eV represents the triple-ionization threshold.

Figure 1 displays the energy levels of the Ne^+ and Ne^{2+} ions that are involved in the considered Auger cascades. As seen from this figure, triple ionization is not possible if we consider only the configurations outlined in Eqs. (1) and (2), since the energetically highest of the considered Ne^+ levels is well below the triple-ionization threshold.

In contrast to previous computations, in which only a few selected decay paths were considered (cf., e.g., Refs. [5,16]), we here model all the possible decay branches that are outlined in Eqs. (1) and (2) in order to find the dominant decay paths and to account for all major correlation contributions from the various electronic configurations.

We do not include the $1s^2 2s^0 2p^6 n\ell \rightarrow 1s^2 2s^1 2p^4 n'\ell' + e^-$ Auger transitions since, based on our calculated *ab initio* energy levels, the $2s^1 2p^4 n'\ell'$ levels are situated slightly above the $2s^0 2p^6 n\ell$ levels. However, the difference is below the uncertainty of the calculations, so we cannot rule out the existence of these transitions in the observed spectra.

B. Calculation of Auger transition rates

Our calculations are based on the so-called Dirac-Coulomb-Breit Hamiltonian

$$H = \sum_i h_{\rm D}(\boldsymbol{r}_i) + V, \tag{3}$$

where $h_{\rm D}$ denotes the one-electron Dirac operator and V the interelectronic interaction operator, i.e., the sum of the Coulomb and Breit interactions between each pair of electrons,

$$V = V_{\rm C} + V_{\rm B} = \sum_{i<j} \left(\frac{1}{r_{ij}} + b_{ij} \right). \tag{4}$$

Within the framework of Ref. [26], based on the theory of resonant scattering, the Auger amplitude for the decay of an initial N-electron state $\Psi_i(P_i J_i M_i)$ with parity P_i, total angular momentum J_i, and projection of total angular momentum M_i into the $(N-1)$-electron final state $\Psi_f(P_f J_f M_f)$, with the respective quantum numbers P_f, J_f, M_f, is given by

$$V_{i\to f,\kappa} = \langle \Psi_f, \epsilon\kappa; P_t J_t \| H - E \| \Psi_i; P_i J_i \rangle \delta_{P_i P_t} \delta_{J_i J_t} \delta_{M_i M_t}, \tag{5}$$

where $\epsilon\kappa$ designates the partial wave of the ejected electron with kinetic energy ϵ and relativistic angular momentum quantum number κ. The coupling of the final ionic state $\Psi_f(P_f J_f M_f)$ with the partial wave $\epsilon\kappa$ of the continuum electron yields a final scattering state with total parity P_t and angular momentum J_t, M_t.

If the wave functions of the initial and the final states are constructed from a common set of orthonormal orbitals, neither the one-electron operators $h_{\rm D}$ nor the total energy E can contribute to the matrix element $V_{i\to f,\kappa}$ within a single-configuration approximation. This Auger amplitude then purely results from the two-electron interaction operator V. In the AUGER component of the RATIP [27] package, the Auger amplitude is therefore simply calculated as

$$V_{i\to f,\kappa} \approx \langle \Psi_f, \epsilon\kappa; P_t J_t \| V \| \Psi_i; P_i J_i \rangle \, \delta_{P_i P_t} \delta_{J_i J_t} \delta_{M_i M_t}, \tag{6}$$

where the partial waves $\epsilon\kappa$ of the continuum electron are generated as *distorted* waves within the potential of the corresponding final ionic state. From these amplitudes $V_{i\to f,\kappa}$ of all the contributing partial waves, the AUGER program then calculates the Auger transition rate; cf. Ref. [28] for further details.

C. The MCDF method

The bound-state wave functions that are utilized for the computation of the Auger amplitudes are generated by applying the multiconfiguration Dirac-Fock (MCDF) method. Within the MCDF formalism, the atomic state function Ψ_α of an energy eigenstate α is constructed as a linear combination of so-called configuration state functions (CSFs) Φ with well-defined parity P, total angular momentum J, and projection of total angular momentum M:

$$\Psi_\alpha(P J M) = \sum_{i=1}^{n_{\rm c}} c_i(\alpha)\, \Phi(\gamma_i P J M). \tag{7}$$

Here, $n_{\rm c}$ denotes the number of CSFs and $\{c_i(\alpha)\}$ is the representation of the atomic state within the given CSF basis. Moreover, γ_i refers to all remaining quantum numbers that are needed to uniquely specify a CSF. Usually, all $n_{\rm c}$ CSFs are constructed from a common set of orthonormal atomic orbitals, i.e., from a set with $\langle \phi_i | \phi_j \rangle = \delta_{ij}$ for each pair of orbitals.

D. Shake processes and the biorthonormal transformation

In order to model the first step of the cascade realistically, we have to consider shake processes of the initially excited np electron into shells with other principal quantum numbers n',

$$1s^1 2s^2 2p^6 np \to 1s^2 2s^k 2p^{6-k} n'\ell + e^-. \tag{8}$$

In a simple picture, shake processes arise from the *overlap* of the different orbitals when the initial and final states are optimized separately. In this model, a shake-up of the valence electron from $3p$ to $4p$ requires that the $3p$ orbital of the initial state overlaps with the $4p$ orbital of the final state. In zeroth approximation, the shake probability is equal to the modulus squared of this orbital overlap, while the mixing between different configurations may lead to additional contributions to the shake probabilities.

Since the initial and the final bound-state wave functions Ψ_i, Ψ_f differ in their number of electrons, the two orbital sets $\{\phi_i\}$ and $\{\phi'_i\}$ of the initial and final states are generally *not* biorthonormal; i.e., the relation $\langle \phi_i | \phi'_j \rangle = \delta_{ij}$ does not hold. While the separately optimized single-electron orbitals are utilized within the AUGER program, this component of the RATIP package still assumes a common orthonormal set of orbitals for both the initial and the final states in the evaluation of the (angular part of the) many-electron Auger amplitudes. Therefore, in order to treat shake processes within the RATIP code, one has to account for the overlap of the initial- and final-state orbitals in a different way, for instance, by employing the biorthonormal transformation as described in Ref. [29] and implemented in the (more recent) GRASP [30] package.

In a *biorthonormal transformation*, the two sets of bound-state orbital functions are modified, $\{\phi_i\}, \{\phi'_i\} \mapsto \{\tilde{\phi}_i\}, \{\tilde{\phi}'_i\}$, such that the obtained orbitals finally fulfill the standard relation $\langle \tilde{\phi}_i | \tilde{\phi}'_j \rangle = \delta_{ij}$. The continuum orbitals are not included in the biorthonormal transformation. Instead, they are generated to be orthogonal to the transformed orbitals of the final ionic state. Of course, any change of the bound-state orbitals also modifies the CSFs, $\Phi(\gamma_i P J M) \mapsto \tilde{\Phi}(\gamma_i P J M)$, and, hence, the representation of the atomic states in the given basis. Therefore, in order to leave the atomic state functions invariant, the coefficients $c_i \mapsto \tilde{c}_i$ need to be transformed as well to fulfill the equivalence

$$\sum_{i=1}^{n_{\rm c}} c_i(\alpha)\, \Phi(\gamma_i P J M) = \sum_{i=1}^{n_{\rm c}} \tilde{c}_i(\alpha)\, \tilde{\Phi}(\gamma_i P J M). \tag{9}$$

By applying a biorthonormal transformation to the atomic states, the (original) orbital overlap is now accounted for by means of the mixing of different configurations and, thus, such a transformation provides a very elegant method to deal with atomic shake processes.

III. CALCULATIONS

The suite of GRASP [30] programs was employed to generate all bound-state wave functions and to perform the biorthonormal transformation of the initial and final states for each step of the cascades. For such a biorthonormal set of orbitals, the Auger decay rates are calculated with the AUGER component of the RATIP package.

To simulate the electron spectra below, the initial resonant photoexcitation as well as all subsequent Auger electron emissions are treated as independent steps of the overall autoionization process. In particular, here we *do not* account for the alignment of the atoms due to their photoexcitation since we are only interested in the (angle-integrated) electron spectra. This is in contrast to a few recent studies on the *coherence* transfer through two (or more) overlapping resonances, and how such a transfer affects the angular distribution of the second-step Auger electrons [15,20].

In the present study, moreover, we do also not consider any *direct* multiple Auger processes which would lead to the simultaneous emission of two or more electrons. These direct processes only occur in second- or even higher-order perturbation theory and are assumed to be negligible as long as sequential Auger cascades are energetically possible. We also neglect all radiative decay processes which are typically suppressed by several orders of magnitude.

A. Bound-state wave function generation

As mentioned before, the first step of the cascade is strongly affected by shake-up or -down processes of the initially excited np ($n = 3,4$) electron into shells with principal quantum numbers $n' \neq n$. In our computations, we have therefore taken into account all those configurations in which the np valence electron is displaced into one of the neighboring $n'p$ orbitals. In the wave function expansions of the intermediate and final states of the cascade, we included all $2\ell^k np$ configurations with $n = 3,\ldots,7$. Further configurations with even higher principal quantum numbers of the spectator electron were found negligible in a series of test computations. In a recent experiment by Tamenori and Suzuki [8], moreover, the *conjugate* shake processes $1s^{-1}3p \rightarrow 1s^2 2s^2 2p^4(^1D)3d$ have also been observed. We therefore also included the $3d$ orbitals in our computations to account for such conjugate shake processes.

Electron correlation effects are known to play an essential role in describing (inner-shell) excited atomic states. For this reason, we have also incorporated various states that cannot be populated during the cascade process (i.e., Ne^{2+} states whose energies are higher than the highest considered Ne^+ state) into the basis, because they often mix with the energetically low-lying states and, hence, may affect the computation of the corresponding Auger rates. To model the relevant states of neutral, singly ionized, as well as doubly ionized neon, we include all CSFs of the following configurations in our computations:

(1) Ne (24 CSFs): $1s^1 2s^2 2p^6 n\ell$ [31],

(2) Ne^+ (261 CSFs): $1s^2 2s^2 2p^5$, $1s^2 2s^1 2p^6$, $1s^2 2s^2 2p^4 n\ell$, $1s^2 2s^1 2p^5 n\ell$, $1s^2 2s^0 2p^6 n\ell$,

(3) Ne^{2+} (516 CSFs): $1s^2 2s^2 2p^4$, $1s^2 2s^1 2p^5$, $1s^2 2s^2 2p^3 n\ell$, $1s^2 2s^0 2p^6$, $1s^2 2s^1 2p^4 n\ell$, $1s^2 2s^0 2p^5 n\ell$, where $n\ell \in \{3p,3d,4p,5p,6p,7p\}$.

B. Energy levels

The second step of the cascade includes a large number of Auger transitions with quite low energies. In order to correctly reproduce these low-energy spectra, one needs to be able to distinguish between the energetically allowed and the energetically forbidden transitions. The level energies from such *ab initio* calculations as performed here are usually not accurate enough to make this distinction explicit. Therefore, we here make use of the experimentally known level energies of neutral, singly, and doubly charged neon, as far as available, to better reproduce the (Auger) energies of the emitted electrons. In some more detail, these experimental energies were obtained from different sources:

(1) Energies of low-lying levels of Ne^+ (where available) and Ne^{2+} as well as the ionization energies were obtained from the NIST Atomic Spectra Database [32].

(2) The Auger spectra from Refs. [7,8,16,17,33] were used for determining some additional Ne^+ energy levels that are not available from optical data.

(3) Values for the $1s^{-1}3p$ and $1s^{-1}4p$ excitation energies were taken from Ref. [25].

For other levels, unfortunately, there is no experimental data available. Nevertheless, these level energies can still be *improved* by using the known energies of neighboring levels and applying a proper interpolation scheme.

IV. RESULTS

We now present the results of our simulation of the complete two-step Auger cascades following the resonant photoexcitation of the core-excited $1s^{-1}3p\ ^1P_1$ and $1s^{-1}4p\ ^1P_1$ levels of neutral neon. We aim to accurately predict the Auger electron spectra, the shake probabilities, as well as the ion yields.

A. The first-step single-ionization spectrum

The resonantly excited $1s^{-1}np\ ^1P_1$ levels can decay to any of the 261 levels of Ne^+ which we consider above in Eq. (1). Here, we shall restrict our discussion to the dominant *peaks* of the calculated spectra, which may consist of one or several Auger transitions between (nearly degenerate) fine-structure levels. Figure 2 shows the calculated Auger electron spectra for the first step of the cascade. For the sake of simplicity, we plot every electron line as a Gaussian with a constant full width at half maximum (FWHM) of 100 meV. Only peaks with a relative intensity >0.01 (with regard to the largest peak in each spectrum) are numbered in the figure and listed in Table I.

The peaks in the spectra of Fig. 2 form several well-separated groups which are associated with different configurations of the Ne^+ ions as listed in Eq. (1). Going from low to high electron energies, we can distinguish the levels of the following final-state configurations for this first step of the cascade: transitions to levels of the $2s^0 2p^6 n\ell$ configurations at 746–756 eV, $2s^1 2p^5 n\ell$ at 770–790 eV, $2s^2 2p^4 n\ell$ at 799–816 eV, $2s^1 2p^6$ at 818.7 eV, as well as to $2s^2 2p^5$ at 845.5–845.6 eV. All these electron energies refer to the decay of the $1s^{-1}3p$ resonance and are released in step (1) of the cascade. For the decay of the $1s^{-1}4p\ ^1P_1$

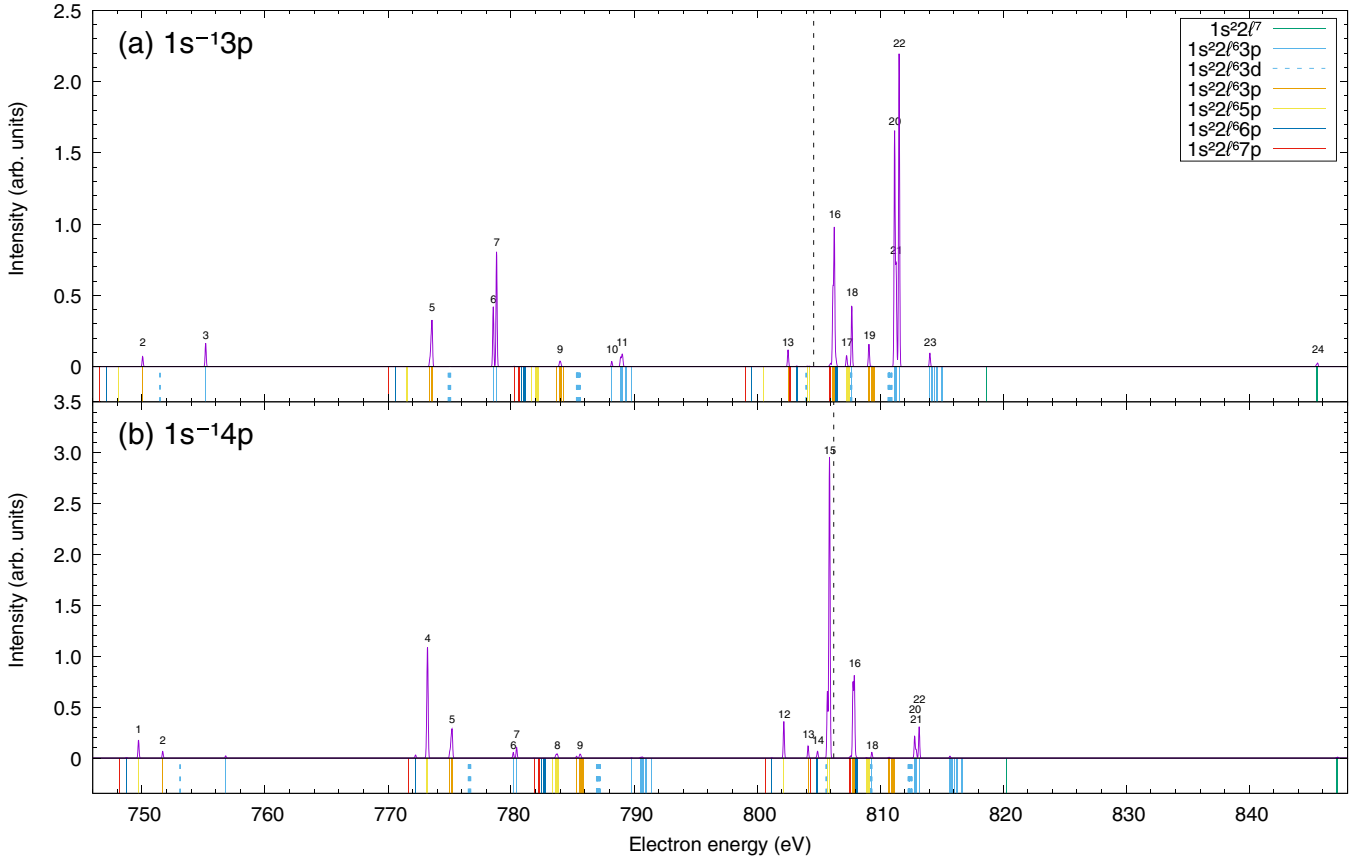

FIG. 2. Simulated Auger electron spectra for the first step (1) of the cascade due to the decay of the core-excited (a) $1s^{-1}3p\,{}^1P_1$ and (b) $1s^{-1}4p\,{}^1P_1$ levels. Every electron line is plotted as a Gaussian with a constant 100 meV FWHM. Peaks with a sufficiently large intensity are labeled with the same numbers as used for indexing in the first column of Table I. The vertical lines below the plots indicate all possible electron transitions in this cascade, where the colors correspond to different final-state configurations; cf. the legend. The two vertical lines at (a) 804.6 eV and (b) 806.2 eV represent the double-ionization threshold. The spectral lines to the left of these dashed lines represent transitions to singly ionized levels with energies above the Ne^{2+} ground state that typically take part in the second step of the cascade.

level, the Auger transitions to the same final levels of Ne^+ yield electron energies that are about 1.6 eV higher owing to the energy difference between the $1s^{-1}3p$ and $1s^{-1}4p$ levels.

The autoionization of the $1s^{-1}3p\,{}^1P_1$ and $1s^{-1}4p\,{}^1P_1$ core-excited levels to the $2s^12p^6\,{}^2S_{1/2}$ level of singly charged neon ions occurs particularly weak in our computations. For these two Auger lines, the calculated relative intensities are only about 4.7×10^{-6} and 1.2×10^{-6} compared to the largest peaks in the respective spectra. This differs from experimental findings where the transitions to the $2s^12p^6\,{}^2S_{1/2}$ level can be clearly seen in the recorded spectra for both excitations; cf. Ref. [6]. A possible reason for this might be an inadequate expansion of the wave function for this particular level. From an analysis of the calculated energies, the $2s^12p^6\,{}^2S_{1/2}$ level energy is indeed found about 5 eV too high with respect to the neighboring $2s^22p^43p$ levels (as obtained from optical data). This rather large deviation indicates that this $^2S_{1/2}$ level is represented rather poorly within the given basis.

The Auger transitions to various levels of the $2s^22p^4n\ell$ configurations of Ne^+ clearly dominate the electron spectra of the first step (1). Altogether, these Auger lines make up about 75% of the total intensity for the decay of the $1s^{-1}3p\,{}^1P_1$ and $1s^{-1}4p\,{}^1P_1$ core-excited levels. Therefore, these groups of transitions have been explored extensively in the literature [3,5,6,8] and, hence, are well suited for a comparison of our computations with experiment. In Table I, for example, we list the measured intensities by Kivimäki *et al.* [6] for the transitions to the $2s^22p^43p$ states. Since the values in Ref. [6] are normalized such that they add up to 100, we scale them appropriately. Our values compare reasonably well to the experimental intensities. Especially the intensity ratios of the dominant transitions to the $2s^22p^4(^1D)3p$ multiplets show very good agreement.

Figure 3 shows the Auger electron spectra of the transitions to the $2s^22p^4n\ell$ states of Ne^+ in greater detail. We here include recent experimental data from Ref. [8] along with our calculated spectra in order to compare the relative intensities of the recorded electron lines. (Note that since we employ experimental energies in our computations, the transition energies naturally match the experimental values.) In the experiment [8], the Auger electron spectra were observed for both parallel and perpendicular polarization of the incident photon beam with respect to the detector axis to obtain angle-resolved spectra. Since we limit ourselves to a simulation of the (angle-integrated) intensities of the transitions with

TABLE I. Energies and intensities of all major electron lines in the first-step Auger electron spectra of $1s^{-1}np\ ^1P_1$ ($n = 3,4$) excited neon. The (relative) intensities of these peaks are denoted by I_Σ and refer for each initial $1s^{-1}np\ ^1P_1$ level to the most intense peak, i.e., to peak 22 for the initial $1s^{-1}3p$ excitation and to peak 15 for $1s^{-1}4p$. For the decay of the core-excited $1s^{-1}3p\ ^1P_1$ level, the calculated intensities are compared, whenever possible, with experimental data by Kivimäki *et al.* [6]. Columns 4 and 7, moreover, display the relative intensities within each single peak, denoted by I, i.e., the fractions of a particular fine-structure line with regard to the intensity of that peak.

		$1s^{-1}3p$ excitation				$1s^{-1}4p$ excitation		
				I_Σ				
No.	Final level(s)	E_k (eV)	I	This work	Expt. [6]	E_k (eV)	I	I_Σ
1	$2s^0 2p^6 5p\ ^2P$					749.72–749.73	1.0	0.043
2	$2s^0 2p^6 4p\ ^2P$	750.06	1.0	0.032		751.69	1.0	0.016
3	$2s^0 2p^6 3p\ ^2P$	755.18	1.0	0.075				
4	$2s^1 2p^5(^1P)5p\ ^2S_{1/2}$					773.15[a]	0.10	0.320
	$2s^1 2p^5(^1P)5p\ ^2P$					773.19	0.33	
	$2s^1 2p^5(^1P)5p\ ^2D$					773.23	0.56	
5	$2s^1 2p^5(^1P)4p\ ^2S_{1/2}$	773.40[a]	0.10	0.233		775.03[a]	0.13	0.121
	$2s^1 2p^5(^1P)4p\ ^2P$	773.50	0.32			775.13	0.35	
	$2s^1 2p^5(^1P)4p\ ^2D$	773.58–773.59	0.58			775.21–775.22	0.52	
6	$2s^1 2p^5(^1P)3p\ ^2P$	778.56	1.0	0.191		780.19	1.0	0.013
7	$2s^1 2p^5(^1P)3p\ ^2D$	778.82–778.83	0.83	0.369		780.45–780.46	0.87	0.026
	$2s^1 2p^5(^1P)3p\ ^2S_{1/2}$	778.84	0.17			780.47	0.13	
8	$2s^1 2p^5(^3P)5p\ ^2P$					783.61–783.65	0.27	0.020
	$2s^1 2p^5(^3P)5p\ ^2D$					783.68–783.79	0.41	
	$2s^1 2p^5(^3P)5p\ ^4P$					783.73–783.74	0.19	
	$2s^1 2p^5(^3P)5p\ ^4D$					783.74–783.81[a]	0.12	
9	$2s^1 2p^5(^3P)4p\ ^2S_{1/2}$	783.70		0.027		785.33	0.24	0.019
	$2s^1 2p^5(^3P)4p\ ^2P$	783.92–783.97	0.35			785.55–785.60	0.27	
	$2s^1 2p^5(^3P)4p\ ^2D$	783.97–784.03	0.44			785.60–785.66	0.34	
	$2s^1 2p^5(^3P)4p\ ^4P$	783.99–784.05	0.17			785.62–785.68	0.13	
	$2s^1 2p^5(^3P)4p\ ^4D$	784.06–784.14[a]	0.03			785.69–785.77[a]	0.02	
10	$2s^1 2p^5(^3P)3p\ ^2S_{1/2}$	788.19	1.0	0.016				
11	$2s^1 2p^5(^3P)3p\ ^2P$	788.89–788.92	0.37	0.081				
	$2s^1 2p^5(^3P)3p\ ^2D$	789.01–789.06	0.58					
	$2s^1 2p^5(^3P)3p\ ^4P$	789.07–789.10[b]	0.05					
12	$2s^2 2p^4(^1S)5p\ ^2P$					802.18	1.0	0.088
13	$2s^2 2p^4(^1S)4p\ ^2P$	802.52	1.0	0.053		804.15	1.0	0.029
14	$2s^2 2p^4(^1D)6p\ ^2P$					804.84[a]	0.09	0.019
	$2s^2 2p^4(^1D)6p\ ^2D$					804.90	0.32	
	$2s^2 2p^4(^1D)6p\ ^2F$					804.93	0.59	
15	$2s^2 2p^4(^1D)5p\ ^2P$					805.71–805.72[a]	0.16	1.0
	$2s^2 2p^4(^1D)5p\ ^2D$					805.86	0.34	
	$2s^2 2p^4(^1D)5p\ ^2F$					805.91	0.50	
16	$2s^2 2p^4(^3P)7p$	805.85–805.99[a]	0.02	0.721		807.48–807.62[a]	0.02	0.381
	$2s^2 2p^4(^1D)4p\ ^2D$	806.17	0.30			807.80	0.32	
	$2s^2 2p^4(^1D)4p\ ^2P$	806.16–806.18	0.03			807.79–807.81	0.15	
	$2s^2 2p^4(^1D)4p\ ^2F$	806.28	0.60			807.91	0.50	
	$2s^2 2p^4(^3P)6p$	806.38–806.50[b]	0.05			808.01–808.13[b]	0.02	
17	$2s^2 2p^4(^3P)5p\ ^2P$	807.26–807.29	0.96	0.038				
	$2s^2 2p^4(^3P)5p\ ^2D$	807.36–807.45	0.01					
	$2s^2 2p^4(^3P)5p\ ^4D$	807.38–807.47	0.02					
18	$2s^2 2p^4(^1S)3p\ ^2P$	807.70	1.0	0.192	0.321	809.33	1.0	0.014
19	$2s^2 2p^4(^3P)4p\ ^2P$	809.07–809.10	1.0	0.075				
20	$2s^2 2p^4(^1D)3p\ ^2D$	811.18	1.0	0.744	0.725	812.81	1.0	0.052

TABLE I. (*Continued.*)

		$1s^{-1}3p$ excitation				$1s^{-1}4p$ excitation		
				I_Σ				
No.	Final level(s)	E_k (eV)	I	This work	Expt. [6]	E_k (eV)	I	I_Σ
21	$2s^2 2p^4(^1D)3p\ ^2P$	811.28–811.31	1.0	0.333	0.373	812.91–812.94	1.0	0.021
22	$2s^2 2p^4(^1D)3p\ ^2F$	811.54–811.55	1.0	1.0	1.0	813.17–813.18	1.0	0.076
23	$2s^2 2p^4(^3P)3p\ ^2P$	814.04–814.05	1.0	0.043	0.027			
24	$2s^2 2p^5\ ^2P$	845.47–845.57	1.0	0.017				

[a]The energies of these transitions are not known from experimental data.
[b]The energies of some of these transitions are not known from experimental data.

no account of the angular distribution, we determine the angle-independent intensities from the experimental data. Our calculated intensities agree well with the experimental spectra. Especially, we can predict quite accurately to which extent shake processes take place and affect the observed spectra.

Table II lists the predicted shake-up and shake-down probabilities for the initially excited $3p$ and $4p$ electrons into neighboring $n\ell$ shells during the first step of the cascade. For an initial $1s^{-1}3p$ excitation, the spectator process that leaves the $3p$ electron in its valence shell clearly dominates with a probability of 72%. For this initial resonance, the shake-up to the $4p$ subshell has a probability of 26%, while the shake-ups into even higher shells are rather weak with respective probabilities <1%. For an initial $1s^{-1}4p$ excitation, in contrast, the shake-up to $5p$ dominates with a probability of 64% over the spectator process (24%). Other notable shake processes are the shake-down to $3p$ (9.6%) and the shake-up to $6p$ (1.5%). Our calculated shake probabilities agree very well with the experimental findings from Ref. [8].

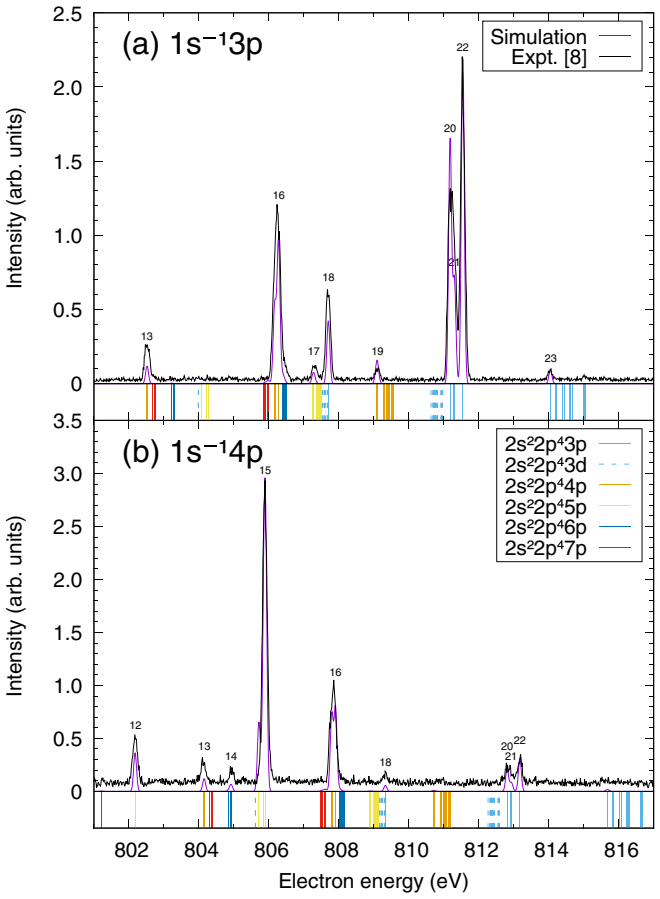

FIG. 3. Comparison of the theoretical and experimental electron spectra. Results from the experiment by Tamenori and Suzuki [8] are shown together with an enlarged part of the simulated spectra from Fig. 2 for (a) the $1s^{-1}3p\ ^1P_1$ and (b) the $1s^{-1}4p\ ^1P_1$ levels.

To predict these shake probabilities, we use the calculated intensities from above and sum over all those intensities that belong to a particular spectator orbital. When we just consider the overall shake probabilities, quite good results (cf., e.g., the calculated values in Ref. [3]) are also obtained by just taking the modulus squared of the orbital overlaps. However, if we need to determine the shake probabilities for some specific transition, this approach is no longer appropriate as one observes significant differences for final levels (terms) that are coupled differently. For example, significant deviations occur for the transitions from the initial $1s^{-1}3p\ ^1P_1$ level to the $2s^2 2p^4(^3P)3p\ ^2P$ and $2s^2 2p^4(^1S)3p\ ^2P$ doublets (peaks 23 and 18) when compared to the corresponding shake-up transitions to the $2s^2 2p^4(^3P)4p\ ^2P$ and $2s^2 2p^4(^1S)4p\ ^2P$ doublets (peaks 19 and 13), respectively. While a shake-up to the $2s^2 2p^4(^3P)4p\ ^2P$ doublet is almost twice as likely as the spectator decay to the $2s^2 2p^4(^3P)3p\ ^2P$ doublet (0.075 : 0.043; cf. Table I), a shake-up to the $2s^2 2p^4(^1S)4p\ ^2P$ doublet is 4 times *less* likely compared to the transitions to the corresponding $2s^2 2p^4(^1S)3p\ ^2P$ doublet (0.053 : 0.192).

According to our calculations, the population of the $3d$ subshell via a conjugate shake process is strongly suppressed

TABLE II. Calculated shake probabilities for the first step of the cascade. Recent experimental values obtained by Tamenori and Suzuki [8] are given for comparison.

Final	$1s^{-1}3p$ excitation		$1s^{-1}4p$ excitation	
orbital	This work	Expt. [8]	This work	Expt. [8]
$3p$	0.72	0.69	0.096	0.08
$3d$	2.9×10^{-4}		5.6×10^{-5}	
$4p$	0.26	0.31	0.24	0.26
$5p$	0.0099	<0.01	0.64	0.64
$6p$	0.0085	<0.01	0.015	0.02
$7p$	0.0036	<0.01	0.0033	<0.01

TABLE III. Calculated ion yields for the decay of the resonantly excited Ne $1s^{-1}np\ ^1P_1$ levels ($n = 3,4$) and comparison with experimental values obtained by Morgan *et al.* [34].

Charge	$1s^{-1}3p$ excitation		$1s^{-1}4p$ excitation	
state	This work	Expt. [34]	This work	Expt. [34]
Ne^+	0.74	0.65(02)	0.24	0.24(03)
Ne^{2+}	0.26	0.31(02)	0.76	0.71(04)
Ne^{3+}		0.03(01)		0.04(01)
Ne^{4+}		0.002		0.002

and almost negligible. In Ref. [8], however, the small peak at 807.3 eV in the $1s^{-1}3p$ spectrum (peak 17 in Fig. 3) has been assigned to the $1s^{-1}3p \rightarrow 2s^22p^4(^1D)3d$ transitions. Based on our computations, we instead propose that the observed peak belongs to the $1s^{-1}3p \rightarrow 2s^22p^4(^3P)5p$ (normal) shake transitions. The calculated intensity of the $(^3P)5p$ transitions exceeds that of the $(^1D)3d$ transitions by about two orders of magnitude, and also the well-known energies of the $2s^22p^4(^1D)3d$ and $(^3P)5p$ levels (as obtained from optical data [32]) suggest that the observed electron lines correspond to the $2s^22p^4(^3P)5p$ levels of the Ne^+ ions.

In Fig. 2, the dashed vertical lines represent the double-ionization threshold. All Auger transitions with an electron energy higher than this threshold populate Ne^+ levels that lie energetically below the Ne^{2+} ground level and, hence, cannot autoionize further. On the other hand, all electron lines below this threshold correspond to autoionizing Ne^+ levels which may decay to Ne^{2+} via one of the second-step transitions listed in Eq. (2). The relative ion yields for Ne^+ and Ne^{2+} are therefore given (in very good approximation) by the intensity ratio of all peaks above and below the threshold. Table III displays the calculated ion yields. The large difference between the ion yields for the $1s^{-1}3p$ and $1s^{-1}4p$ excitations arises mainly from the different population of the $2s^22p^4(^1D)5p$ levels in the first step of the cascade. These levels lie 0.3–0.5 eV above the double ionization threshold and are dominantly populated in the first-step Auger decay following the $1s^{-1}4p$ excitation, while their population is negligible for an initial $1s^{-1}3p$ excitation. Our results for the ion yields agree quite satisfyingly with the experimental data by Morgan *et al.* [34] which are shown for comparison in Table III. While triply and even quadruply charged neon ions have been observed in the experiment [34], they require higher-order processes, such as direct double and triple Auger electron emissions or shake-up processes of two or more electrons, and are thus not included in the present study.

B. The second-step double-ionization spectrum

The second-step Auger electron spectra span the energy range between 0 and 59 eV and comprise a total of 1512 transitions between fine-structure levels of Ne^+ and Ne^{2+}. About 800 of these lines have low electron energies (<10 eV).

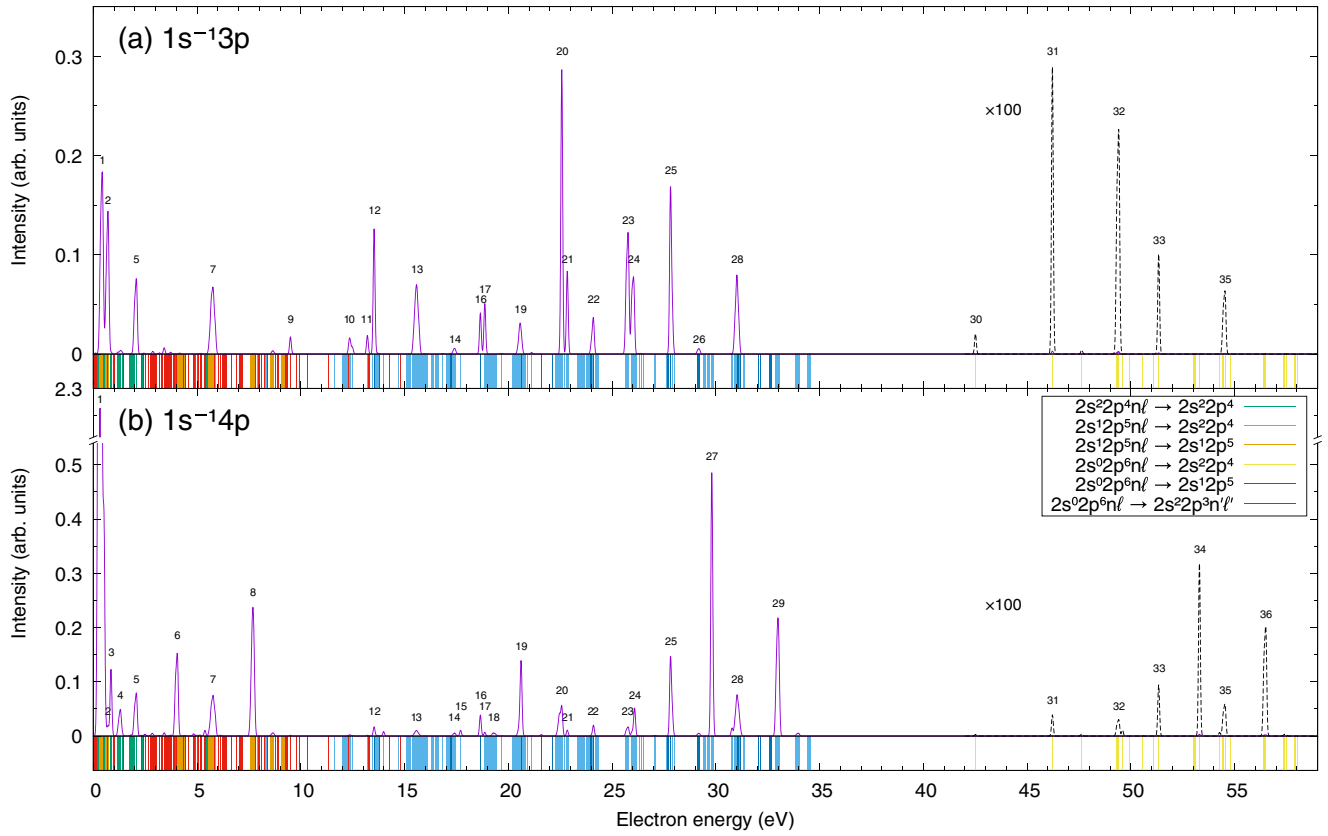

FIG. 4. The same as Fig. 2 but for the second step (2) of the Auger cascade. Peaks with a sufficiently large intensity are labeled again with numbers that refer to the numbers in the first columns of Tables IV, V, and VI. The colors of the vertical lines below the plots correspond to different initial and final configurations as shown in the legend. For electron energies higher than 42 eV, the peaks are enhanced by a factor of 100 to make the $2s^02p^6n\ell \rightarrow 2s^22p^4$ transitions visible.

TABLE IV. The same as in Table I but for the second-step Auger electron lines with energies between 0–8 eV. Here, the relative intensities I_Σ refer to peaks 20 + 21 for the $1s^{-1}3p$ excitation and to peak 27 for $1s^{-1}4p$; cf. Table V.

				$1s^{-1}3p$		$1s^{-1}4p$	
No.	Initial level(s)	Final level(s)	E_k (eV)	I	I_Σ	I	I_Σ
1	$2s^22p^4(^1D)5p\,^2F$	$2s^22p^4\,^3P$	0.21–0.33		0.793	0.50	7.901
	$2s^22p^4(^1D)5p\,^2D$	$2s^22p^4\,^3P$	0.26–0.37	0.01		0.34	
	$2s^12p^5(^1P)3p\,^2S_{1/2}$	$2s^12p^5\,^3P$	0.32–0.43	0.46			
	$2s^12p^5(^1P)3p\,^2D$	$2s^12p^5\,^3P$	0.34–0.45	0.51		0.01	
	$2s^22p^4(^1D)5p\,^2P$	$2s^22p^4\,^3P$	0.40–0.52[a]	0.01		0.16	
2	$2s^02p^66p\,^2P$	$2s^22p^3(^2P)3d\,^3P$	0.64–0.66		0.568	0.01	0.053
	$2s^12p^5(^1P)3p\,^2P$	$2s^12p^5\,^3P$	0.60–0.72	1.0		0.99	
3	$2s^22p^4(^1S)5p\,^2P$	$2s^22p^4\,^1D_2$	0.85			0.99	0.235
	$2s^02p^64p\,^2P$	$2s^22p^3(^2P)3p\,^1S_0$	0.86			0.01	
4	$2s^22p^4(^1D)6p\,^2F$	$2s^22p^4\,^3P$	1.19–1.31			0.58	0.146
	$2s^22p^4(^1D)6p\,^2D$	$2s^22p^4\,^3P$	1.22–1.33			0.32	
	$2s^22p^4(^1D)6p\,^2P$	$2s^22p^4\,^3P$	1.28–1.40[a]			0.09	
5	$2s^22p^4(^1S)6p\,^2P$	$2s^22p^4\,^1D_2$	1.82		0.318	0.01	0.236
	$2s^02p^65p\,^2P$	$2s^22p^3(^2D)3d\,^1F_3$	1.84			0.01	
	$2s^22p^4(^1S)4p\,^2P$	$2s^22p^4\,^3P$	1.97–2.09	1.0		0.96	
	$2s^02p^65p\,^2P$	$2s^22p^3(^2D)3d\,^1P_1$	2.07			0.02	
6	$2s^22p^4(^1S)5p\,^2P$	$2s^22p^4\,^3P$	3.94–4.06			1.0	0.458
7	$2s^12p^5(^1P)4p\,^2D$	$2s^12p^5\,^3P$	5.58–5.69	0.23	0.408	0.18	0.320
	$2s^02p^65p\,^2P$	$2s^22p^3(^2P)3p\,^3S_1$	5.69			0.02	
	$2s^12p^5(^1P)4p\,^2P$	$2s^12p^5\,^3P$	5.66–5.77	0.44		0.41	
	$2s^12p^5(^1P)4p\,^2S_{1/2}$	$2s^12p^5\,^3P$	5.76–5.87[a]	0.32		0.39	
8	$2s^12p^5(^1P)5p\,^2D$	$2s^12p^5\,^3P$	7.56–7.67			0.21	0.744
	$2s^12p^5(^1P)5p\,^2P$	$2s^12p^5\,^3P$	7.60–7.72			0.44	
	$2s^12p^5(^1P)5p\,^2S_{1/2}$	$2s^12p^5\,^3P$	7.64–7.76[a]			0.35	

[a]The energies of these Auger lines are not known from experimental data.

Figure 4 displays the calculated Auger electron spectra for step (2) of the cascade, taking into account the relative population of the initial states after step (1). Large parts of these spectra have been explored before with emphasis on different aspects [8,16,17]. While the dominant peaks are all situated below 35 eV, some additional peaks occur in the range between 42 and 59 eV. In the following, we shall therefore separately discuss three parts of the spectrum with energies 0–8 eV, 8–35 eV, and 42–59 eV, respectively.

Table IV lists all the significant peaks with energies below 8 eV together with their relative intensities. This part of the spectra is dominated by so-called *multiplet-changing Auger transitions* [35] in which the energy required for the release of the Auger electron does not arise from a change in the shell occupation (electron configuration) but from the coupling of different terms of the remaining ion, i.e., a change of the multiplet coupling of the underlying parent state. For this reason, the Auger electrons in these transitions are typically emitted with very low energy. In the second step (2) of the neon cascade, the following multiplet-changing transitions are energetically allowed: The $2s^22p^4(^1D)5p$, $(^1D)6p$, $(^1D)7p$, $(^1S)3d$, and $(^1S)4p$ states of Ne^+ can decay to the $2s^22p^4\,^3P$ states of Ne^{2+}, while the $2s^22p^4(^1S)5p$, $(^1S)6p$, and $(^1S)7p$ states can decay to the $2s^22p^4\,^3P$ and $^1D_2$ states. Furthermore, all of the considered $2s^12p^5(^1P)n\ell$ states can decay to the $2s^12p^5\,^3P$ states.

In addition to the multiplet-changing transitions, many of the $2s^02p^6n\ell \rightarrow 2s^22p^3n'\ell'$ shake transitions also lie in this energy range. In further detail, the energetically allowed final states here include all of the $2s^22p^33p$ and $2s^22p^33d$ states as well as the $2s^22p^3(^4S)4p$ and $2s^22p^3(^4S)5p$ states; cf. Fig. 1 above. As expected, these transitions are generally very weak, since, in addition to the low population of the $2s^02p^6n\ell$ levels, these second-step transitions require a conjugate shake-down $2p \rightarrow 2s$ and are, hence, strongly suppressed compared to the normal Auger transitions to the $2s^12p^5$ levels. These transitions are therefore hard to detect as they occupy just the same energy region as the comparatively strong multiplet-changing transitions. Until now, these shake-down transitions have not been observed experimentally. Nevertheless, some of the peaks in Table IV show some minor contributions from these lines.

The intensities I_Σ of the peaks listed in Table IV are given relative to the total intensity of the two peaks 20 and 21 for the $1s^{-1}3p$ excitation and relative to peak 27 for the $1s^{-1}4p$ excitation. We have chosen this normalization for the $1s^{-1}3p$ peaks because we wish to compare the intensities for the 8–35 eV energy range with experimental values which are normalized the same way. In order to be still able to compare the intensities of peaks from different energy ranges, we shall use these peaks above for normalizing the whole second-step spectra. Although, for the initial $1s^{-1}4p$ excitation, peak 1

TABLE V. The same as in Table IV but for the second-step Auger electron lines with energies between 8–35 eV. For the $1s^{-1}3p$ excitation, the relative intensities measured by Yoshida *et al.* [16] are shown for comparison.

				$1s^{-1}3p$				$1s^{-1}4p$	
				This work		Expt. [16]			
No.	Initial level(s)	Final level(s)	E_k (eV)	I	I_Σ	I	I_Σ	I	I_Σ
9	$2s^1 2p^5(^3P)3p\ ^2S_{1/2}$	$2s^2 2p^4\ ^1S_0$	9.50	1.0	0.046				
10	$2s^1 2p^5(^3P)3p\ ^4P$	$2s^2 2p^4\ ^1D_2$	12.30–12.32[b]	0.03	0.072	0.02(02)	0.22(02)		
	$2s^1 2p^5(^3P)3p\ ^2D$	$2s^2 2p^4\ ^1D_2$	12.34–12.39	0.72		0.49			
	$2s^1 2p^5(^3P)3p\ ^2P$	$2s^2 2p^4\ ^1D_2$	12.48–12.51	0.25		0.39(13)			
11+12	$2s^1 2p^5(^3P)3p\ ^2S_{1/2}$	$2s^2 2p^4\ ^1D_2$	13.21	0.13	0.395	0.16(01)	0.58(04)	0.07	0.038
	$2s^0 2p^6 3p\ ^2P$	$2s^1 2p^5\ ^1P_1$	13.53	0.86		0.80(04)		0.86	
	$2s^1 2p^5(^3P)4p\ ^4P$	$2s^2 2p^4\ ^1S_0$	13.64–13.70			n/a[d]		0.02	
	$2s^1 2p^5(^3P)4p\ ^2D$	$2s^2 2p^4\ ^1S_0$	13.66–13.72	0.01		n/a[d]		0.04	
	$2s^1 2p^5(^3P)4p\ ^2P$	$2s^2 2p^4\ ^1S_0$	13.72–13.77			n/a[d]		0.01	
13	$2s^1 2p^5(^3P)3p\ ^4P$	$2s^2 2p^4\ ^3P$	15.39–15.53[b]	0.05	0.401		0.44(03)	0.05	0.040
	$2s^1 2p^5(^3P)3p\ ^2D$	$2s^2 2p^4\ ^3P$	15.43–15.60	0.55		0.8[c]		0.50	
	$2s^1 2p^5(^3P)5p\ ^4D$	$2s^2 2p^4\ ^1S_0$	15.51–15.58[a]					0.01	
	$2s^1 2p^5(^3P)5p\ ^4P$	$2s^2 2p^4\ ^1S_0$	15.58–15.59					0.02	
	$2s^1 2p^5(^3P)5p\ ^2D$	$2s^2 2p^4\ ^1S_0$	15.53–15.64					0.06	
	$2s^1 2p^5(^3P)3p\ ^2P$	$2s^2 2p^4\ ^3P$	15.57–15.71	0.40		0.4[c]		0.35	
	$2s^1 2p^5(^3P)5p\ ^2P$	$2s^2 2p^4\ ^1S_0$	15.67–15.71					0.01	
14+15	$2s^0 2p^6 3d\ ^2D$	$2s^1 2p^5\ ^1P_1$	17.24	0.04	0.024	n/a[d]	0.12(01)		0.036
	$2s^1 2p^5(^3P)4p\ ^4D$	$2s^2 2p^4\ ^1D_2$	17.25–17.34[a]	0.01		n/a[d]			
	$2s^1 2p^5(^3P)4p\ ^4P$	$2s^2 2p^4\ ^1D_2$	17.35–17.41	0.15		0.09(01)		0.07	
	$2s^1 2p^5(^3P)4p\ ^2D$	$2s^2 2p^4\ ^1D_2$	17.36–17.43	0.42		0.31(02)		0.21	
	$2s^1 2p^5(^3P)7p\ ^2S_{1/2}$	$2s^2 2p^4\ ^1S_0$	17.42[a]	0.09		n/a[d]		0.01	
	$2s^1 2p^5(^3P)4p\ ^2P$	$2s^2 2p^4\ ^1D_2$	17.42–17.48	0.27		0.30(02)		0.13	
	$2s^1 2p^5(^3P)4p\ ^2S_{1/2}$	$2s^2 2p^4\ ^1D_2$	17.70	0.01		0.08(01)		0.57	
16+17	$2s^0 2p^6 4p\ ^2P$	$2s^0 2p^5\ ^1P_1$	18.65	0.45	0.248	0.98(05)	0.23(02)	0.85	0.087
	$2s^1 2p^5(^1P)3p\ ^2S_{1/2}$	$2s^2 2p^4\ ^1S_0$	18.85	0.01		n/a[d]			
	$2s^1 2p^5(^1P)3p\ ^2D$	$2s^2 2p^4\ ^1S_0$	18.86–18.87	0.54		n/a[d]		0.15	
18	$2s^1 2p^5(^3P)5p\ ^4D$	$2s^2 2p^4\ ^1D_2$	19.22–19.29[a]					0.09	0.020
	$2s^1 2p^5(^3P)5p\ ^4P$	$2s^2 2p^4\ ^1D_2$	19.28–19.30					0.20	
	$2s^1 2p^5(^3P)5p\ ^2D$	$2s^2 2p^4\ ^1D_2$	19.24–19.34					0.48	
	$2s^1 2p^5(^3P)5p\ ^2P$	$2s^2 2p^4\ ^1D_2$	19.38–19.41					0.23	
19	$2s^1 2p^5(^3P)4p\ ^4D$	$2s^2 2p^4\ ^3P$	20.34–20.54[a]	0.03	0.137		0.22(02)	0.01	0.316
	$2s^1 2p^5(^3P)4p\ ^4P$	$2s^2 2p^4\ ^3P$	20.44–20.61	0.17		0.1[c]		0.05	
	$2s^1 2p^5(^3P)4p\ ^2D$	$2s^2 2p^4\ ^3P$	20.45–20.63	0.43		0.4[c]		0.13	
	$2s^1 2p^5(^3P)6p\ ^2S_{1/2}$	$2s^2 2p^4\ ^1D_2$	20.55	0.01					
	$2s^1 2p^5(^3P)4p\ ^2P$	$2s^2 2p^4\ ^3P$	20.51–20.68	0.36		0.6[c]		0.11	
	$2s^0 2p^6 5p\ ^2P$	$2s^1 2p^5\ ^1P_1$	20.62					0.69	
20+21	$2s^1 2p^5(^3P)5p\ ^4P$	$2s^2 2p^4\ ^3P$	22.37–22.50		1.0		1.0	0.11	0.226
	$2s^1 2p^5(^3P)5p\ ^4D$	$2s^2 2p^4\ ^3P$	22.31–22.50[a]					0.08	
	$2s^1 2p^5(^3P)5p\ ^2D$	$2s^2 2p^4\ ^3P$	22.33–22.55					0.23	
	$2s^1 2p^5(^3P)5p\ ^2P$	$2s^2 2p^4\ ^3P$	22.47–22.62					0.16	
	$2s^1 2p^5(^1P)3p\ ^2D$	$2s^2 2p^4\ ^1D_2$	22.57–22.58	0.77		0.94(05)		0.33	
	$2s^1 2p^5(^1P)3p\ ^2P$	$2s^2 2p^4\ ^1D_2$	22.84	0.23		0.06(01)		0.09	
22	$2s^0 2p^6 3p\ ^2P$	$2s^1 2p^5\ ^3P$	23.98–24.10	0.58	0.133	1.0[c]	0.22(02)	0.17	0.042
	$2s^1 2p^5(^1P)4p\ ^2D$	$2s^2 2p^4\ ^1S_0$	24.10–24.11	0.42				0.82	
	$2s^1 2p^5(^1P)4p\ ^2S_{1/2}$	$2s^2 2p^4\ ^1S_0$	24.29[a]					0.01	
23+24	$2s^1 2p^5(^1P)3p\ ^2D$	$2s^2 2p^4\ ^3P$	25.66–25.78	0.60	0.860	0.3[c]	0.85(05)	0.30	0.170
	$2s^1 2p^5(^1P)3p\ ^2P$	$2s^2 2p^4\ ^3P$	25.93–26.05	0.40		0.7[c]		0.19	
	$2s^1 2p^5(^1P)5p\ ^2D$	$2s^2 2p^4\ ^1S_0$	26.09					0.51	
25	$2s^1 2p^5(^1P)4p\ ^2D$	$2s^2 2p^4\ ^1D_2$	27.81	0.79	0.555	0.97(05)	0.53(04)	0.76	0.353
	$2s^1 2p^5(^1P)4p\ ^2P$	$2s^2 2p^4\ ^1D_2$	27.90	0.21		0.03(01)		0.24	

TABLE V. (*Continued.*)

				$1s^{-1}3p$				$1s^{-1}4p$	
				This work		Expt. [16]			
No.	Initial level(s)	Final level(s)	E_k (eV)	I	I_Σ	I	I_Σ	I	I_Σ
26	$2s^0 2p^6 4p\ ^2P$	$2s^1 2p^5\ ^3P$	29.10–29.22	1.0	0.022	0.9[c]	0.12(01)		
27	$2s^1 2p^5(^1P)5p\ ^2D$	$2s^2 2p^4\ ^1D_2$	29.80					0.79	1.0
	$2s^1 2p^5(^1P)5p\ ^2P$	$2s^2 2p^4\ ^1D_2$	29.84					0.21	
28	$2s^1 2p^5(^1P)6p\ ^2D$	$2s^2 2p^4\ ^1D_2$	30.77		0.370		0.36(03)	0.08	0.318
	$2s^1 2p^5(^1P)6p\ ^2P$	$2s^2 2p^4\ ^1D_2$	30.81					0.02	
	$2s^1 2p^5(^1P)4p\ ^2D$	$2s^2 2p^4\ ^3P$	30.90–31.02	0.59		0.4[c]		0.42	
	$2s^1 2p^5(^1P)4p\ ^2P$	$2s^2 2p^4\ ^3P$	30.99–31.10	0.41		0.6[c]		0.35	
	$2s^0 2p^6 5p\ ^2P$	$2s^1 2p^5\ ^3P$	31.07–31.18					0.14	
29	$2s^1 2p^5(^1P)5p\ ^2D$	$2s^2 2p^4\ ^3P$	32.89–33.00					0.56	0.677
	$2s^1 2p^5(^1P)5p\ ^2P$	$2s^2 2p^4\ ^3P$	32.93–33.04					0.44	

[a]The energies of these Auger lines are not known from experimental data.
[b]The energies of *some* of these Auger lines are not known from experimental data.
[c]These values are based on the best fit to the observed peak structure and are considered tentative [16].
[d]These intensities cannot be established since the observed peaks are not assigned to a specific transition in Ref. [16].

of the second-step spectrum is apparently the largest, we here choose peak 27 as reference because the spectrum with electron energies >5 eV has been explored earlier in great detail (e.g., Ref. [17]), in contrast to the very low energy part. Peak 27 is taken as reference since it is the largest in this range of kinetic energies above 5 eV.

Unfortunately, it is difficult to assess the accuracy of the calculated intensities for these low-energy transitions. Previous experimental studies have investigated this low-energy part; e.g., Refs. [8,17]. While these experimental findings agree very well with our computations for the identification of the dominant peaks in the spectra (apart from peak 2; cf. below), no quantitative analysis has been performed so far for the intensity ratios between these peaks.

In Ref. [8], the lines with energies of 0.60–0.72 eV in the second-step spectra (peak 2 in our spectra) have been attributed to the $2s^2 2p^4(^1S)3d \rightarrow 2s^2 2p^4\ ^3P$ transitions. Since the $2s^2 2p^4(^1S)3d$ levels are populated only marginally during the first step, these transitions are very weak in our simulated spectra. Based on the analysis of both steps of the cascade, we propose that the observed peaks likely belong to the $2s^1 2p^5(^1P)3p \rightarrow 2s^1 2p^5\ ^3P$ transitions instead, since the computed intensity of these transitions exceeds that of the $2s^2 2p^4(^1S)3d \rightarrow 2s^2 2p^4\ ^3P$ transitions by five orders of magnitude. Energies for the $2s^1 2p^5(^1P)3p$ levels are not known from optical data but can be derived from the data in Ref. [33] under the assumption that the assignments in this reference (which were obtained by comparing the measured branching ratios and anisotropy parameters with MCDF calculations) are correct. Using these values for the $2s^1 2p^5(^1P)3p$ energies, one obtains Auger electron energies between 0.32 and 0.72 eV for the $2s^1 2p^5(^1P)3p \rightarrow 2s^1 2p^5\ ^3P$ transitions, which fits well the experimentally observed peaks.

In the higher-energy part of the second-step spectra, the $2s^1 2p^5 n\ell \rightarrow 2s^2 2p^4$ and $2s^0 2p^6 n\ell \rightarrow 2s^1 2p^5$ Auger transitions dominate in the range from 8 to 35 eV. At energies below 15 eV, also some of the $2s^1 2p^5(^1P)n\ell \rightarrow 2s^1 2p^5\ ^3P$ and $2s^0 2p^6 n\ell \rightarrow 2s^2 2p^3 n'\ell'$ transitions occur, but with rather small contributions. For this part of the spectra, the energies

TABLE VI. The same as in Table IV but for the second-step Auger electron lines with energies between 42–59 eV.

				$1s^{-1}3p$		$1s^{-1}4p$	
No.	Initial level(s)	Final level(s)	E_k (eV)	I	I_Σ	I	I_Σ
30	$2s^0 2p^6 3p\ ^2P$	$2s^2 2p^4\ ^1S_0$	42.51	1.0	0.000 55		
31	$2s^0 2p^6 3p\ ^2P$	$2s^2 2p^4\ ^1D_2$	46.21–46.22	1.0	0.007 81	1.0	0.000 74
32	$2s^0 2p^6 3p\ ^2P$	$2s^2 2p^4\ ^3P$	49.30–49.42	1.0	0.009 73	0.81	0.001 14
	$2s^0 2p^6 5p\ ^2P$	$2s^2 2p^4\ ^1S_0$	49.59–49.60			0.19	
33	$2s^0 2p^6 4p\ ^2P$	$2s^2 2p^4\ ^1D_2$	51.34	1.0	0.002 72	1.0	0.001 79
34	$2s^0 2p^6 5p\ ^2P$	$2s^2 2p^4\ ^1D_2$	53.30			1.0	0.006 09
35	$2s^0 2p^6 6p\ ^2P$	$2s^2 2p^4\ ^1D_2$	54.27		0.002 71	0.06	0.001 91
	$2s^0 2p^6 4p\ ^2P$	$2s^2 2p^4\ ^3P$	54.43–54.54	1.0		0.94	
36	$2s^0 2p^6 5p\ ^2P$	$2s^2 2p^4\ ^3P$	56.39–56.51			1.0	0.006 08

and relative intensities are listed in Table V and compared with the experiment from Ref. [16] for the initial $1s^{-1}3p$ excitation. Good quantitative agreement is found between experiment and simulations for all dominant transitions in the $1s^{-1}3p$ spectrum. In Ref. [16], however, the peaks $11+12$, $14+15$, $16+17$, $20+21$, and $23+24$ were grouped together and, hence, we here provide the combined intensities of these peaks in Table V. For some of the *weak* peaks, the simulated and experimental intensities deviate up to a factor 5, especially for the peaks 10, $14+15$, and 26. For the $1s^{-1}4p$ excitation, we find good qualitative agreement with the recorded spectrum from Ref. [17].

Table V also compares the intensity ratios I of the individual Auger lines with experimental data whenever possible. Although the fine structure of the ^3P multiplets was resolved in the experiment [16], we here present the combined intensities of the transitions to the ^3P levels in order to keep the size of Table V feasible. In practice, however, the comparison with the experimental intensities I is not always simple as no assignments were made for some of the observed peaks. We denote these cases by "n/a" in Table V. For some other peaks, moreover, the intensity ratios of the contributing transitions cannot be resolved and were just estimated by a fit. The uncertainties of these intensities are believed to be of the order of the reported values [16]. These values are quoted in Table V for the sake of completeness and are marked appropriately. While very good agreement is found especially for peaks $11+12$ and $14+15$, some larger deviations occur for other peaks. This applies especially to the peaks 16 and 17, which have similar intensities in our computations, while peak 16 clearly dominates experimentally.

The spectrum between 42–59 eV comprises the $2s^02p^6n\ell \rightarrow 2s^22p^4$ transitions. These transitions are generally weak when compared with the decay to the $2s^12p^5$ levels and are two orders of magnitude less intense than the major peaks at 8–35 eV. This behavior is expected since these transitions include a conjugate shake-down $2p \rightarrow 2s$, similar to the $2s^02p^6n\ell \rightarrow 2s^22p^3n'\ell'$ transitions. They have not yet been observed experimentally. In order to make them visible in our simulated spectrum in Fig. 4, they are enlarged by a factor of 100. The transitions that make up the labeled peaks are listed in Table VI.

From the analysis of the electron spectra, we can also derive the population of final states of each step of the cascade. For the first step, the relative population of final Ne^+ levels can be directly obtained from the (computed) Auger rates since the initial $1s^{-1}np\ ^1P_1$ level is the same for all transitions. For the second step of the cascade, in contrast, the rather large number of *initial* states then leads to a final-state distribution that is less obvious. Figure 5 shows the relative population of the energy levels of Ne^{2+} after the second step of the cascade. Moreover, Table VII lists the relative population per fine-structure multiplet for the $2s^22p^4$ and $2s^12p^5$ levels, and just per configuration for the (less populated) $2s^22p^3n\ell$ levels. Experimentally, such a final-state distribution is obtained quite easily if all the emitted electrons are recorded in coincidence, like in a magnetic bottle; cf., e.g., Ref. [18] for a recent study of triple ionization of atomic cadmium.

The second step (2) of the cascades leads with a probability of >99% to one of the levels of the $2s^22p^4$ or $2s^12p^5$ configuration. Since the higher-lying $2s^22p^3n\ell$ levels can only be populated via the rare $2s^02p^6n\ell \rightarrow 2s^22p^3n'\ell'$ transitions, their population remains almost negligible. Out of these $2p^22p^3n\ell$ levels, several $3p$ and $3d$ levels are predominantly

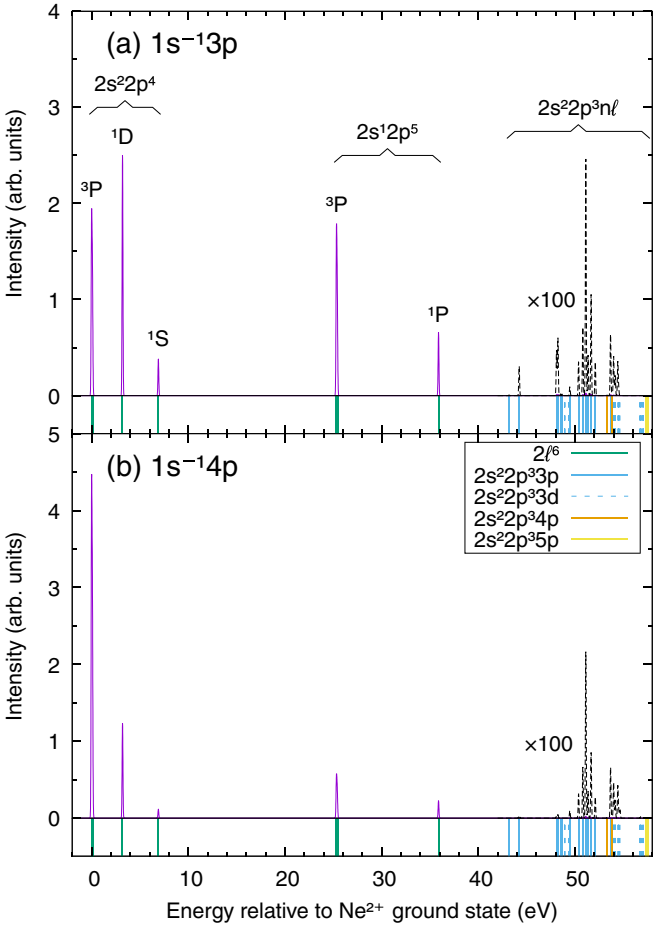

FIG. 5. Simulated population of the Ne^{2+} energy levels for the (a) $1s^{-1}3p\ ^1P_1$ and (b) $1s^{-1}4p\ ^1P_1$ excitations. The part of the spectra that belongs to the $2s^22p^3n\ell$ levels is enhanced by a factor of 100 in order to make the population of these levels visible.

TABLE VII. Relative population of the final Ne^{2+} energy levels after the second step (2) of the cascade. The energies are given relative to the Ne^{2+} $2s^22p^4\ ^3P_2$ ground level.

		Relative population	
Level(s)	Energy (eV)	$1s^{-1}3p$	$1s^{-1}4p$
$2s^22p^4\ ^3P$	0.00–0.11	0.33	0.73
$2s^22p^4\ ^1D_2$	3.20	0.27	0.13
$2s^22p^4\ ^1S_0$	6.91	0.040	0.012
$2s^12p^5\ ^3P$	25.33–25.44	0.29	0.093
$2s^12p^5\ ^1P_1$	35.89	0.070	0.024
$2s^22p^33p$	43.20–53.69	0.0080	0.0059
$2s^22p^33d$	48.93–57.40	0.0011	0.0014
$2s^22p^3(^4S)4p$	53.32–53.85	4.1×10^{-5}	3.0×10^{-5}
$2s^22p^3(^4S)5p$	57.34–57.51	5.0×10^{-9}	5.5×10^{-8}

populated, while the population of the $2s^2 2p^3(^4S)4p\ ^{3,5}P$ and $2s^2 2p^3(^4S)5p\ ^{3,5}P$ levels is energetically allowed, but does not occur in practice. It should be noted that the population of doubly ionized states is likely affected by direct double Auger processes, which are not considered in this study. In particular, the experimental ion yields (cf. Table III) suggest that direct double processes lead to the population of autoionizing Ne^{2+} levels and thus to the creation of triply charged neon.

V. CONCLUSION

We have analyzed the two-step Auger cascades following the resonant photoexcitation of the $1s^{-1}3p\ ^1P_1$ and $1s^{-1}4p\ ^1P_1$ core-excited levels in neon. Extensive MCDF calculations have been carried out to incorporate all major correlation contributions in the representation of the initial, intermediate, and final states of the cascade. In addition, we have taken the important (single-electron) shake processes, which are known to play an essential role in describing these Auger cascades, into account. To this end, we applied the biorthonormal transformation to the atomic orbitals and the representation of the separately optimized atomic states. With this approach, we are able to simulate Auger electron spectra and to predict ion yields as well as shake probabilities that are in very good agreement with experiments. So-called conjugate shake processes to the $3d$ subshell are however found to be suppressed by several orders of magnitude compared to the dominating spectator and shake processes in the first step of the cascade. For the second step, we also found the yet unobserved weak decay channels $2s^0 2p^6 n\ell \rightarrow 2s^2 2p^4$ and $2s^0 2p^6 n\ell \rightarrow 2s^2 2p^3 n'\ell'$ which include a conjugate shake-down $2p \rightarrow 2s$.

In conclusion, our theoretical study clearly demonstrates that, apart from selected Auger lines, one can meanwhile simulate whole electron spectra or even (multiple) decay cascades with quite satisfying accuracy. This requires extensive computations with correlated wave functions, for which the MCDF method has been found versatile. While the autoionization of inner-shell excited neon atoms still refers to a rather simple system, we plan to extend these computations towards more complex atoms and/or Auger cascades. A careful theoretical analysis of such cascades may support also ongoing developments of new (magnetic-bottle) coincidence techniques as well as of time- and position-resolved detectors.

ACKNOWLEDGMENTS

We would like to thank Yusuke Tamenori for providing the experimental data from Ref. [8]. This research was funded by the German Federal Ministry of Education and Research (BMBF) under Contract No. 05K16SJA.

[1] T. A. Carlson and M. O. Krause, Phys. Rev. Lett. **14**, 390 (1965).
[2] W. Eberhardt, G. Kalkoffen, and C. Kunz, Phys. Rev. Lett. **41**, 156 (1978).
[3] H. Aksela, S. Aksela, J. Tulkki, T. Åberg, G. M. Bancroft, and K. H. Tan, Phys. Rev. A **39**, 3401 (1989).
[4] H. Aksela, S. Aksela, H. Pulkkinen, A. Kivimäki, and O.-P. Sairanen, Phys. Scr. **41**, 425 (1990).
[5] Y. Shimizu, H. Yoshida, K. Okada, Y. Muramatsu, N. Saito, H. Ohashi, Y. Tamenori, S. Fritzsche, N. M. Kabachnik, H Tanaka, and K. Ueda, J. Phys. B **33**, L685 (2000).
[6] A. Kivimäki, S. Heinäsmäki, M. Jurvansuu, S. Alitalo, E. Nõmmiste, H. Aksela, and S. Aksela, J. Electron Spectrosc. Relat. Phenom. **114–116**, 49 (2001).
[7] A. De Fanis, G. Prümper, U. Hergenhahn, E. Kukk, T. Tanaka, M. Kitajima, H. Tanaka, S. Fritzsche, N. M. Kabachnik, and K. Ueda, J. Phys. B **38**, 2229 (2005).
[8] Y. Tamenori and I. H. Suzuki, J. Phys. B **47**, 145001 (2014).
[9] Y. Hikosaka, T. Kaneyasu, P. Lablanquie, F. Penent, E. Shigemasa, and K. Ito, Phys. Rev. A **92**, 033413 (2015).
[10] J. Viefhaus, A. N. Grum-Grzhimailo, N. M. Kabachnik, and U. Becker, J. Electron Spectrosc. Relat. Phenom. **141**, 121 (2004).
[11] S. Schippers, A. Borovik, Jr., T. Buhr, J. Hellhund, K. Holste, A. L. D. Kilcoyne, S. Klumpp, M. Martins, A. Müller, S. Ricz, and S. Fritzsche, J. Phys. B **48**, 144003 (2015).
[12] A. Müller, A. Borovik, Jr., T. Buhr, J. Hellhund, K. Holste, A. L. D. Kilcoyne, S. Klumpp, M. Martins, S. Ricz, J. Viefhaus, and S. Schippers, Phys. Rev. Lett. **114**, 013002 (2015).
[13] M. Ya. Amusia, I. S. Lee, and V. A. Kilin, Phys. Rev. A **45**, 4576 (1992).
[14] F. Zhou, Y. Ma, and Y. Qu, Phys. Rev. A **93**, 060501(R) (2016).
[15] H. Yoshida, K. Ueda, N. M. Kabachnik, Y. Shimizu, Y. Senba, Y. Tamenori, H. Ohashi, I. Koyano, I. H. Suzuki, R. Hentges, J. Viefhaus, and U. Becker, J. Phys. B **33**, 4343 (2000).
[16] H. Yoshida, J. Sasaki, Y. Kawabe, Y. Senba, A. De Fanis, M. Oura, S. Fritzsche, I. P. Sazhina, N. M. Kabachnik, and K. Ueda, J. Phys. B **38**, 465 (2005).
[17] M. Kitajima, H. Yoshida, A. De Fanis, G. Prümper, U. Hergenhahn, E. Kukk, T. Tanaka, K. Nakagawa, H. Tanaka, S. Fritzsche, I. P. Sazhina, N. M. Kabachnik, and K. Ueda, J. Phys. B **39**, 1299 (2006).
[18] J. Andersson, R. Beerwerth, P. Linusson, J. H. D. Eland, V. Zhaunerchyk, S. Fritzsche, and R. Feifel, Phys. Rev. A **92**, 023414 (2015).
[19] S. Schippers, R. Beerwerth, L. Abrok, S. Bari, T. Buhr, M. Martins, S. Ricz, J. Viefhaus, S. Fritzsche, and A. Müller, Phys. Rev. A **94**, 041401(R) (2016).
[20] F. Da Pieve, L. Avaldi, R. Camilloni, M. Coreno, G. Turri, A. Ruocco, S. Fritzsche, N. M. Kabachnik, and G. Stefani, J. Phys. B **38**, 3619 (2005).
[21] A. G. Kochur, A. I. Dudenko, V. L. Sukhorukov, and I. D. Petrov, J. Phys. B **27**, 1709 (1994).
[22] A. G. Kochur, V. L. Sukhorukov, A. I. Dudenko, and Ph. V. Demekhin, J. Phys. B **28**, 387 (1995).
[23] A. G. Kochur and V. L. Sukhorukov, J. Phys. B **29**, 3587 (1996).
[24] A. G. Kochur and Ye. B. Mitkina, J. Phys. B **32**, L41 (1999).
[25] M. Kato, Y. Morishita, M. Oura, H. Yamaoka, Y. Tamenori, K. Okada, T. Matsudo, T. Gejo, I. H. Suzuki, and N. Saito, AIP Conf. Proc. **879**, 1121 (2007).

[26] T. Åberg and G. Howat, in *Corpuscles and Radiation in Matter I*, edited by S. Flügge and W. Mehlhorn, Encyclopedia of Physics Vol. 31 (Springer-Verlag, Berlin and Heidelberg, 1982), pp. 469–619.

[27] S. Fritzsche, Comput. Phys. Commun. **183**, 1525 (2012).

[28] S. Fritzsche, B. Fricke, and W.-D. Sepp, Phys. Rev. A **45**, 1465 (1992).

[29] J. Olsen, M. R. Godefroid, P. Jönsson, P. Å. Malmqvist, and C. Froese Fischer, Phys. Rev. E **52**, 4499 (1995).

[30] P. Jönsson, X. He, C. Froese Fischer, and I. P. Grant, Comput. Phys. Commun. **177**, 597 (2007).

[31] These 24 CSFs refer to all possible CSFs of the $1s^{-1}n\ell$ configurations ($n\ell \in \{3p,3d,4p,5p,6p,7p\}$). Because of their angular momentum and parity, only the 10 CSFs belonging to the $1s^{-1}np\ ^{1,3}P_1$ levels can actually mix into the initial $1s^{-1}3p\ ^1P_1$ and $1s^{-1}4p\ ^1P_1$ states. The $1s^{-1}3d$ states are included nevertheless because the biorthonormal transformation as well as the AUGER program require that the initial and final state basis sets contain equivalent orbitals.

[32] A. Kramida, Yu. Ralchenko, J. Reader, and NIST ASD Team, NIST Atomic Spectra Database, Version 5.4, 2016, http://physics.nist.gov/asd

[33] K. Ueda, M. Kitajima, A. De Fanis, Y. Tamenori, H. Yamaoka, H. Shindo, T. Furuta, T. Tanaka, H. Tanaka, H. Yoshida, R. Sankari, S. Aksela, S. Fritzsche, and N. M. Kabachnik, Phys. Rev. Lett. **90**, 153005 (2003).

[34] D. V. Morgan, M. Sagurton, and R. J. Bartlett, Phys. Rev. A **55**, 1113 (1997).

[35] U. Becker, O. Hemmers, B. Langer, I. Lee, A. Menzel, R. Wehlitz, and M. Ya. Amusia, Phys. Rev. A **47**, R767(R) (1993).